IJASRM

International Journal of Advanced Scientific Research and Management, Volume 3 Issue 8, Aug 2018

www.ijasrm.com

ISSN 2455-6378

Spectroscopic (FTIR, FT-Raman And NMR) Investigations and NBO Analysis of 2-Hydroxybenzothiazole By Quantum Mechanical Technique

Rasheed .M.P[1] ,S Seshadri [2],R sangeetha[3], Satheeshkumar M.K[4]

[1,3]Research Scholar, PG and Research Department of Physics,
Urumudhanalakshmi College ,Trichy-19, India

[2]Associate Professor and HOD,PG and Research Department of Physics,
Urumudhanalakshmi College ,Trichy-19, India

[4]Associate professor and Head (Rtd),Govt. Brennen College,
Thalassery, Kannur, Kerala, India

Abstract

This work explains vibrational spectroscopic characteristics of 2-Hydroxybenzothiazole (2HBT) with the help of quantum mechanical calculations. The Fourier Transform Infra Red (FTIR) spectra of 2-Hydroxybenzothiazole was and recorded in the region 4000-400 cm^{-1} and that of Fourier Transform Raman Spectra (FT-Raman) spectra was recorded in the region 4000-50 cm^{-1}. The optimized geometry, intensity and different frequency of the vibrational bands were calculated by the density functional theory (DFT) using B3LYP/6-311++ G (d,p) basis set. Molecular Electrostatic Potential map of the compound was analyzed. The harmonic vibrational frequencies were obtained and the scaled frequencies have been compared with experimental FTIR and FT-Raman spectra. The experimental and calculated frequencies were found to be in good agreement. Thermodynamic properties at different temperatures were performed, giving the relation between heat capacity, entropy and enthalpy with temperatures. The ^{1}H and ^{13}C Nuclear Magnetic Resonance (NMR) were studied using the GIAO method by applying B3LYP technique. Mullikan atomic charges were listed.NBO analysis were performed. The hyper conjugative interaction energy and electron densities of the donor and acceptor bond were studied by NBO analysis

Keywords: *DFT,FTIR,FT-RAMAN,NMR, NBO,2HBT.*

1. Introduction

Benzothiazole is an is an aromatic heterocyclic compound with the chemical formula C_7H_5NS. It consists of a five membered 1,3, thiazole fused to a benzene ring. It is a colourless and slightly viscous liquid. Many of the derivatives of benzothiazole are found in commercial products or in nature. A derivative of benzothiazole is the light emitting component of luciferin which found in fireflies. Benzothiazole are prepared by treatment of 2-mercaptoaniline with acid chloride [T. E. Gilchrist,1992]. It is thermally stable electron withdrawing moiety with various applications in dyes such as thioflavin. Some drugs contain this group for example riluzole and pramipexole [Lucille Le Bozec et al]. It exhibits thioredoxine inhibitory activity. 2 mercaptobenzothiazole is used as accelators for the vulcanization of rubber [Hans-Wilhelm Engels et al, 2004]. It is a potential component in nonlinear optics (NLO) [P.Hrobarik et al 2010]. This compound is also used as food flavouring agent and insecticide.

2. Experimental Details

The finest sample of 2HBT was obtained from Sigma Aldrich Chemical Company UK and used as such for the spectroscopic analysis. Using a BRUCKER IFS-66V vacuum Fourier Transform

Spectrometer equipped with a Mercury Cadmium Telluride (MCT) detector and a KBr beam splitter global source, the FTIR spectrum of the compound 2HBT was measured in the region 4000-400 cm^{-1} at a resolution of ±1 cm^{-1}.

The FT-Raman spectra was also recorded in the range between 4000 and 50 cm^{-1} by the instrument with FRA 106 Raman module equipped with Nd:YAG laser source with 200 mW power operating at 1.064 nm. The reported wave numbers are expected to be accurate within ±1 cm^{-1}.

3. Computational Details

The Density Functional Theory (DFT) has been proved to be extremely useful in treating electronic structure of molecules. The entire calculations (vibrational wavenumbers, geometric parameters, and other molecular properties) were calculated and analysed by using GaussView 5.0 program [Roy Dennington et al 2009] and Gaussian 09W program package on a computing system [M. J. Frisch et al 2009] . Additionally, the calculated vibrational frequencies were explained by means of the potential energy distribution (PED) analysis of all the fundamental vibration modes. The potential energy distributions corresponding to each of the observed frequencies were calculated with the help of MOLVIB-7.0 program [T. Sundius,1990,T.Sundius 2002]. Normal coordinate analysis on 2HBT has been performed to obtain full description of the molecular motion pertaining to the normal modes.

The intensities of Raman scattering depend on the square of the infinitesimal change of the polarizability with respect to the normal coordinates. Normal coordinate specifies the instantaneous displacement of an independent mode of oscillation of the system. Each normal coordinate oscillates at a characteristic frequency and is completely unaffected by the other coordinates. For a specific vibration mode *i*, its Raman activity (S_i) and Raman intensity (I_i) are two different quantities. Raman activity is a intrinsic property of each molecular vibrational mode, while Raman intensity is directly related to experimental Raman spectrum, and its value is dependent of the choice of wavenumber of incident light ν_0 as well as temperature

The Raman activities (S_i) calculated by Gaussian 09 program have been suitably adjusted by the scaling procedure with MOLVIB and subsequently converted to relative Raman intensities (I_i) using the following relationship derived from the basic theory of Raman scattering [G. Keresztury et al1993, G. Keresztury et al 2002]

$$I_i = \frac{f(\nu_0-\nu_i)^4 S_i}{\nu_i\left[1-exp\left(\frac{-hc\nu_i}{kT}\right)\right]} \qquad (1)$$

where ν_0 is the exciting frequency (in cm^{-1} units); ν_i is the vibrational wave number of the i^{th} normal mode; *h*, *c* and *k* are fundamental constants and f is a suitably chosen common normalization factor for all peaks intensities.

4. Results and discussion

4.1 Molecular Geometry

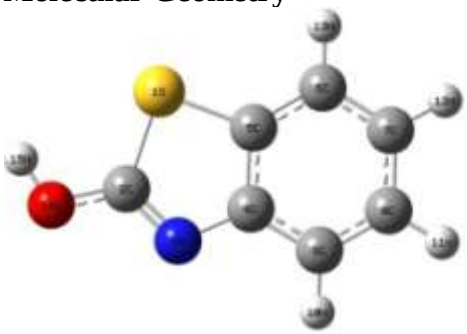

Fig 1. Optimized Structure of 2HBT along with numbering of atoms

The optimized molecular structure and the labelling of atoms of title compound is obtained from Gaussian 09W and Gauss View 5.0 programs are shown in Figure. 1. The global minimum energies obtained by the DFT structure optimization for 2HBT for B3LYP/6-31G (d,p) , B3LYP/6-31+G(d,p), and B3LYP/6-311+G (d,p) basis sets respectively are presented in Table 1. This energy difference may be due to the molecules are under different environments.

Table 1-Total energies (in Hartrees) based on different basis sets for 2HBT

Basis set	2HBT
B3LYP/6-31G(d,p)	-797.9289
B3LYP/6-31+ G(d,p)	-797.9471
B3LYP/6-311+ G(d,p)	-798.0564

angles from molecule to molecule depending upon on the electron structures of the molecule.

A dihedral angle or torsion angle is the angle between two planes. The optimized geometrical parameters like bond length, bond angles and dihedral angles are calculated and listed in Table 2.

The two important parameters which determine the shape and size of a molecule are bond length and bond angles. By analyzing the bond length and bond angle we can characterize the geometry of a molecule. Bond angles vary in their

IJASRM
International Journal of Advanced Scientific Research and Management, Volume 3 Issue 8, Aug 2018
www.ijasrm.com
ISSN 2455-6378

Table 2-Optimized geometrical parameters of 2HBT obtained by B3LYP/6-311+ g(d,p) density functional calculations

Bond	Angstrum (Å)	Bond angle	Degree	Torsional angle	Degree
S1-C5	1.762006	C5-C6-C7	117.97	H15-O14-C2-S1	0.04
C8-C7	1.401036	S1-C5-C6	129.01	H13-C6-C7-C8	-180.02
C4-C9	1.397818	H15-O14-C2	111.01	H12-C7-C8-C9	-179.98
C7-C6	1.392689	H13-C6-C7	120.75	H11-C8-C9-C4	-179.98
C5-C6	1.391553	H12-C7-C6	119.38	H10-C9-C8-C7	-180.01
C9-C8	1.389997	H11-C8-C9	119.51	C2-N3-C4-C5	-0.01
N3-C4	1.388041	H10-C9-C8	121.61	C5-C6-C7-C8	-0.02
O14-C2	1.342913	C2-N3-C4	110.78	C9-C8-C7-C6	0.02
N3-C2	1.278113	C9-C8-C7	121.03	C4-C9-C8-C7	0.01
C8-H11	1.083844	C4-C9-C8	119.16	O14-S1-N3-C2	0
C7-H12	1.083695	C8-C7-C6	120.79	S1-C4-C6-C5	0.01
C6-H13	1.083258	O14-C2-N3	122.34	N3-C5C9-C4	0.01
C9-H10	1.083113	N3-C4-C9	125.1		
O14-H15	0.963466				

For numbering of atoms refer Fig. 1

4.2 Analysis of Molecular Electrostatic Surface Potential

An electron density isosurface mapped with electrostatic potential surface depicts the size, shape, charge density and site of chemical reactivity of the molecules. It provides a visual method to understand the relative polarity of the molecule [S. Chidangil et al 1998, F.J. Luque et al 2000]. Molecular electrostatic potential shown in Figure 10 illustrates the charge distributions of the molecule 2HBT three dimensionally. The molecular electrostatic surface (MESP) provides a visual method to understand the relative polarity of the compounds [A.E. Reed et al 1985]. Electrostatic potential map shown in Fig. 2 illustrates the charge distributions of the molecule three dimensionally. Knowledge of the charge distributions can be used to determine how molecules interact with one another. One of the purposes of finding the electrostatic potential is to find the reactive site of a molecule [J.M. Seminario et al 1996, R.H. Petrucci et al 2007]. In the electrostatic potential map, the semi-spherical blue shapes that emerge from the edges of the above electrostatic potential map are hydrogen atoms. Molecular electrostatic potential (MEP) at a point in space around a molecule gives information about the net electrostatic effect produced at that point by total charge distribution (electron + proton) of the molecule and correlates with dipole moments, electro negativity, partial charges and chemical reactivity of the molecules. The molecular electrostatic potential (MEP) at a point r in the space around a molecule (in atomic units) can be expressed as

$$V(r) = \sum_A \frac{Z_A}{|R_A - r|} - \int \frac{\rho(r')}{|r' - r|} dr' \quad (2)$$

Where Z_A is the charge of nucleus A located at R_A, $\rho(r')$ is the electronic density function of the molecule, and r' is the dummy integration variable. The first and second term represent the contributions to the potential due to nuclei and electron respectively. V(r) is the net resultant electrostatic effect produced at the point r by both the electrons and nuclei of the molecule. The different values of the electrostatic potential at the surface are represented by different colours. The red colour represents regions of most electronegative electrostatic potential, blue colour represents regions of the most positive electrostatic potential and green colour represents regions of zero potential . Potential increases in the order red < orange < yellow < green < blue [V. Balachandran et al 2012]. Blue indicates the strongest attraction and red indicates the strongest repulsion. Regions of negative potential are usually associated with the lone pair of electronegative atoms [Y. Sheena Mary et al 2015] . As can be seen from the MEP map of the title molecule, negative region are mainly localized over nitrogen in the ring and oxygen atom in the nitro grou p. That is negative potential sites are on the electronegative atoms while the positive potential sites around the hydrogen and carbon atoms. The maximum positive region is localized on the hydrogen atom of amino group. Green area covers parts of the molecule where electrostatic potentials are nearly equal to zero (C-C bond). This is a region of zero potential enveloping the π systems of aromatic ring leaving a more electrophilic region in

IJASRM
International Journal of Advanced Scientific Research and Management, Volume 3 Issue 8, Aug 2018
www.ijasrm.com
ISSN 2455-6378

the plane of hydrogen atom. The electrostatic potential contour map of positive and negative potential is shown in Figure 3

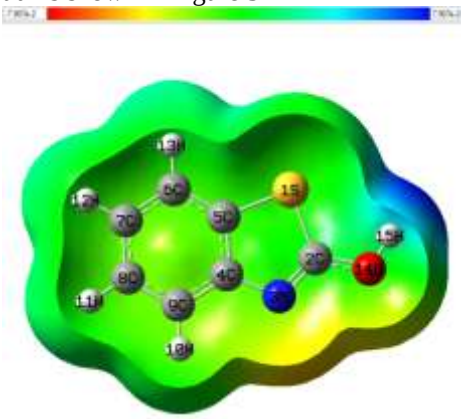

Fig 2. Total electron density isosurface mapped with molecular electrostatic potential of 2HBT

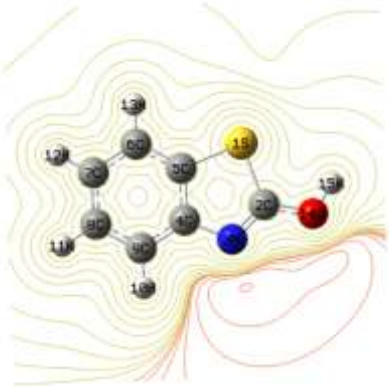

Fig 3. Contour map of molecular electrostatic potential surface

4.3 Assignment of spectra

Theoretical and experimental FT-IR spectrum of 2HBT is given in Figure 4

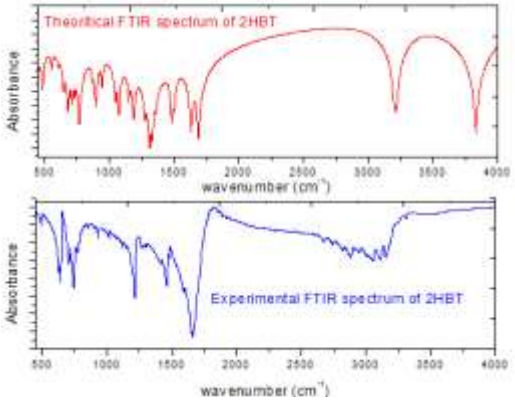

Fig 4. Comparison of Theoretical and experimental FT-IR spectrum of 2HBT

Theoretical and experimental FT Raman spectrum of 2HBT is given in Figure 5. Comparison between the calculated and observed vibrational spectra helps us to understand the observed spectralfeatures

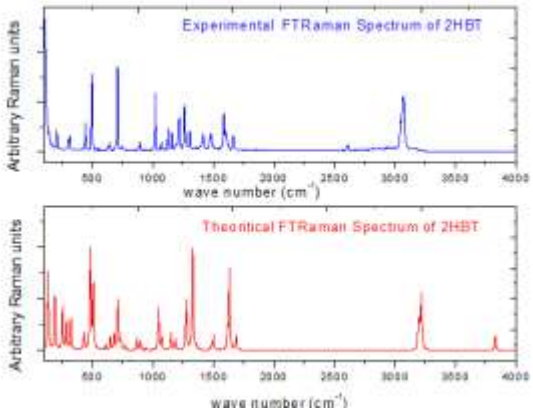

Fig 5. Comparison of Experimental and Theoretical FT-Raman spectrum of 4A3NP

The vibrations of a molecule are given by its normal modes. Each absorption in a vibrational spectrum corresponds to a normal mode. Detailed description of vibrational modes can be given by means of normal coordinate analysis and it also gives a complete picture about the molecular dynamics of compound. Non-linear molecules have three rotational axes, hence 3N-6 normal modes. Our title molecule belongs to C_1 point group symmetry and consists of 15 atoms, which undergo 39 normal modes of vibrations .The total number of 39 fundamental vibrations are distributed as Γ_{vib} 39 = 27 A' (In plane vibrations) + 12 A" (out of plane vibrations). The A' modes be polarized while the A" modes be depolarized in the Raman spectra of the liquid. The results of our vibrational analysis, viz., calculated unscaled vibrational frequencies and IR intensities, Scaled Quantum Mechanical (SQM) frequencies, potential energy distributions (PED) and assignment of the fundamentals, for the title compound were collected and tabulated in Table 3 .

When using computational methods to predict theoretical normal vibrations for relatively complex poly atomic structures, scaling strategies are used to bring computed wave numbers into closer agreement with observed frequencies using the latest version of MOLVIB program.

IJASRM

International Journal of Advanced Scientific Research and Management, Volume 3 Issue 8, Aug 2018

www.ijasrm.com

ISSN 2455-6378

TABLE 3 - Assignment of fundamental vibrations of 2HBT by normal mode analysis based on SQM force field calculations using selective scaled B3LYP/6-31g(d,p)

No	symmetry species	Observed frequency		Calculated using B3LYP/6-31 G(d,p) force field Freq					Characterisation of normal modes with PED%
		IR (cm^{-1})	Raman (cm^{-1})	Unscaled (cm^{-1})	Scaled (cm^{-1})	IR intensity (K mol^{-1})	Raman activity S_i	Raman intensity (I_i)	
1	A'	-	-	3834.9	3418	106.873	114.90	109.77	vOH (100)
2	A'	3279	-	3200.0	2873	8.2487	262.07	466.48	vCH (99)
3	A'	-	-	3193.2	2866	16.8078	90.17	161.63	vCH (99)
4	A'	3155	-	3182.4	2857	9.1129	106.83	193.62	vCH (99)
5	A'	3133	3070.96	3171.0	2846	1.5793	50.20	92.05	vCH (99)
6	A'	1661	1664.47	1664.1	1621	170.282	14.57	167.87	bCH (47), vCC (39)
7	A'	-	-	1610.5	1598	90.3194	84.08	1053.55	bCH (67), vCC (31)
8	A'	-	1598.28	1599.7	1570	3.5034	24.62	313.78	bCH (81), vCC (13)
9	A'	-	1480.69	1488.4	1555	15.9803	12.19	186.29	bCH (31), vNC (23), vCC (23)
10	A'	1472	-	1468.9	1512	45.7328	4.86	76.72	vNC (30), bCH (26), vCC (16)
11	A'	-	-	1343.4	1354	13.6838	2.80	55.11	bCH (32), vCC (30), R5b2 (12)
12	A'	1311	-	1319.6	1314	178.67	78.04	1603.61	vCC (40), bCH (35),
13	A'	-	1306.05	1298.3	1288	348.703	1.64	34.97	COH (45), vCO (15), bCH (10)
14	A'	1265	1262.09	1263.2	1211	29.6283	37.34	852.81	vNC (28), bTri (25), vCC (18),
15	A'	-	-	1182.9	1178	20.0732	1.74	46.42	vCC (88),
16	A'	-	1154.45	1171.7	1133	21.3919	3.53	96.47	vCC(20), bTri(12), vNC(11), bCC(10),
17	A'	1129	-	1143.7	1112	6.9416	10.07	291.66	vCC (41), vCO (14), vNC (12), bCH (11)
18	A'	-	1071.02	1071.3	1068	24.6535	7.87	265.80	bTri (42), bCC (22), vCC (16)
19	A'	1022	1019.4	1038.3	975	7.5195	29.58	1074.52	vCC (68),
20	**A"**	-	-	988.6	971	0.04	0.01	0.25	oCH (89),
21	**A"**	946	-	949.8	933	2.1909	0.26	11.76	oCH (90),
22	A'	-	889.72	896.2	879	11.9208	3.49	178.06	vCC (32), bTri (18), vCO (10), vNC (10)
23	**A"**	871	-	863.3	863	1.0892	0.30	16.71	oCH (88)
24	**A"**	745	-	762.0	769	50.9261	1.70	125.04	oCH (51), tTri (33)
25	**A"**	-	-	719.3	742	4.3298	0.34	28.61	tTri (50), oCH (39)
26	A'	-	707.42	710.4	698	8.8911	15.04	1293.78	bCC (35), vCS (24), vCC (21)
27	A'	655		680.9	686	17.5371	5.20	491.35	bSym(26), vCC(19), bCH(14), R5b1(12), vCO(12)
28	A'	642	641.65	647.0	646	3.3114	2.04	215.49	vCS (28), bCH (24), R5b1 (19), vCC (10)
29	**A"**	-	-	607.4	622	0.2625	0.84	101.92	oOC (41), R5t2 (37)
30	**A"**	-	-	549.6	568	0.4161	0.03	5.00	tAsym(32), oOC(23), oCH(14), tTri(12), R5t1(10)
31	A'	501	-	506.7	515	0.0124	10.28	1848.26	R5b1(26), R5b2(23), vCS(15), vCC(14), bCC(12)
32	A'	494	498.9	482.5	472	2.9609	15.85	3167.17	vCS(23), bCC(16), vCC(15), vNC(12), bSym(10)
33	**A"**	-	441.18	432.1	448	1.6911	0.05	13.20	tSym (73), oCH (10)
34	A'	-	-	429.2	438	6.1753	2.27	583.24	vCS (33), bCC (33), bCH (19)
35	**A"**	-	313.57	321.0	331	5.0443	0.48	227.45	tAsym(24), tSym(23), R5t2(19), oCH(11)
36	A'	-	-	287.5	298	5.559	1.87	1114.98	bCC (41), vCS (21), bCH (18)
37	**A"**	-	-	232.8	251	114.835	1.23	1139.15	tCO (76), oOC (22)
38	**A"**	-	205.6	184.4	194	0.0805	1.01	1508.35	R5t1 (33), tAsym (31), tCO (10),
39	**A"**	-	106.97	130.7	136	2.945	0.66	1986.74	R5t2 (46),tbutter (13),

(υ) stretching; (b) bending; (o) out of plane ;(t) torsion; (R5) five member Ring,;(Sym) Symmetric;(butter) Butterfly; (Asym) asymmetric ; PED values greater than 10% are given

The RMS error between unscaled (B3LYP/6-311++ g(d,p)) and experimental frequencies are found to be 38.3 cm^{-1}.Root mean square value is obtained in the study using the following expression

$$RMS = \sqrt{\frac{1}{n-1}\sum_i^n (v_i^{calcu} - v_i^{exp})^2} \quad (3)$$

This is quite obvious since the frequencies calculated on the basis of quantum mechanical force fields usually differ appreciably from observed frequencies. This is partly due to neglect of anharmonicity and partly due to the approximate nature of the quantum mechanical methods . In order to reproduce the observed frequencies, refinement of scaling factors are applied and optimized via least square refinement algorithm which resulted in a weighted RMS deviation of 9.65 cm^{-1} between the experimental and scaled frequencies.

For 2HBT, a multiple scale factors are applied in the normal coordinate analysis and the subsequent least square fit refinement, results into the very close agreement between the observed fundamentals and the scaled frequencies (Table 3). Refinement of the scaling factor applied in this study achieved a weighted mean deviation of 5.26 cm^{-1} between the experimental and SQM frequencies. It is beneficial to discuss the vibrational spectra of 2HBT in terms of characteristic spectral regions which are described in detail below.

4.3.1 C-H vibration

The hetero aromatic structure shows the presence of C-H stretching vibrations in the region 3100-3000 cm^{-1} which is the characteristic region [N.B. Colthup et al,1964]. The IR spectrum usually has several bands here while the Raman usually has only one. The 2HBT has four adjacent C –H moieties. In the present study the three expected C-H stretching vibrations correspond to mode Nos. 2, 3, 4 and 5. The bands appear at 3279 cm^{-1}, 3155 cm^{-1} and 3133 cm^{-1} cm^{-1} in IR spectrum were assigned to C-H stretching vibrations The weak band at 3070.7 cm^{-1} in Raman Spectrum has been assigned to C-H stretching vibration.

The bands due to C-H in-plane ring bending vibrations, interacting somewhat with C-C stretching vibrations and C-N vibrations , are observed as a number of medium and weak intensity sharp bands in the region 1600-1000 cm^{-1}.Hence bands observed at 1661 cm^{-1}, 1472 cm^{-1} and 1311 cm^{-1} in IR spectrum and the bands observed at 1664.4 cm^{-1},1598.2 cm^{-1},1480.6 cm^{-1} and 1306 cm^{-1} in Raman spectrum have been assigned to C-H in plane bending vibrations as shown in Table 3. The C-H out-of-plane bending vibrations are strongly coupled vibrations and occur in the region 900-667 cm^{-1}.Hence the band appeared at 946 cm^{-1}, 871 cm^{-1},745 cm^{-1} in IR spectrum were assigned to C-H out of plane bending vibrations.

4.3.2 C-C vibration

In this case there are two rings, a six membered ring and a five membered ring.The ring carbon-carbon stretching vibrations investigation occurs in the region in 1625-1430 cm^{-1} [N. Sundaraganesan et al,2008]. The C-C vibrations are coupled with C-C stretching vibrations.In the present case the bands of C-C stretching vibrations in the two rings appear at 1661 cm^{-1},1472 cm^{-1} and 1311 cm^{-1} in FTIR and 1306 cm^{-1} and 1262 cm^{-1} in Raman spectra are also consistent with the calculated one. These assignments are in good agreement with the literature [M. Arivazhagan et al ,2009].

4.3.3 Ring Vibrations

For aromatic ring, some bands are observed below 700 cm^{-1}. These bands are quite sensitive to change in nature and position of the substituent [R.J. Jakobsen et al 1964, A. Mansingh et al 1970, L. Verdonck et al 1973, L. Verdonck et al 1974].Usually an in-plane deformation vibration is at higher frequencies than the out of plane vibration [A.P. Datin et al ,1969] . In the present study, the bands observed at 655 cm^{-1} in FTIR and 1154.4, 1071.0 and 889.72 cm^{-1} in FT Raman spectrum respectively are attributed to ring in-plane bending modes. The ring out-of-plane bending mode frequencies are established at 745 cm^{-1} in FT Raman and frequencies at 441.18, 313.57 and 205.6 cm^{-1} in FTIR spectra as shown in Table 3

4.3.4 C-N vibrations

The identification of C-N vibration is a very difficult task since mixing of several bands is possible in this region. However, with the help of theoretical calculations, the C-N stretching vibrations are identified and assigned in this study. Silverstein et al. [M. Silverstein et al ,1981] assigned C-N stretching absorption in the region 1382-1266 cm^{-1} for aromatic amines. Pyrimidine absorb strongly in the region 1600-1500 cm^{-1} due to the C-C and C-N ring stretching vibrations. Absorbance is also absorbed at 1640-1620 cm, 1580– 1520 cm, 1000- 960 cm^{-1} and 825-775 cm^{-1}.For the title compound 2HBT the C-N stretching modes are observed at 1480.6 cm^{-1} and 1262.0 in FT Raman spectrum and 1472 cm^{-1} in FTIR spectrum . These vibrations are mixed with C-C stretching and C-H bending vibrations as evident from the last column (PED) of Table 3.

4.3.5 C-S vibration

In general the assignment of the band due to the C-S stretching vibration in different compounds is difficult in the infrared since the band is of variable intensity and may be found over the wide region 1035-245 cm^{-1} .whereas, in general C-S stretching vibrations result in strong bands in Raman spectra which are normally easy to identify [George Socrates,2001] . In this present work, some percentage of the band observed at 642 cm^{-1},501 cm^{-1} in FTIR spectrum and 707.4 cm^{-1} ,641.65 cm^{-1} in Raman spectrum have been attributed to C-N vibrations.

4.3.6 Alcohols group vibration (R-OH)

In the alcohol group bands due to O-H stretching and bending vibrations and C-O stretching vibrations are observed. The relative intensity of the band due to the hydroxyl stretching vibration appearing at frequencies 3580-3200 cm^{-1}. These bands are the result of the presence of intermolecular bonding, the amount of which increases with concentration. The precise position of the O-H band is dependent on the strength of the hydrogen bond. In some samples, intramolecular hydrogen bonding may occur, the resulting hydroxyl group band which appears at 3590-3400 cm^{-1} being sharp and unaffected by concentration changes. For solids, liquids, and concentrated solutions, a broad band is normally observed at about 3300 cm^{-1}. Hydroxyl groups which are hydrogen-bonded to aromatic ring electron systems absorb at 3580-3480cm^{-1} . In the case of our tile compound the FTIR band observed at 3344 cm^{-1} is attributed to O-H stretching vibration.

The absorption region for the alcohol C-O group due to its stretching vibration is 1200-1000 cm^{-1}. The COC stretching band at 1090-1000 cm^{-1} is characteristic of primary alcohols. In this case COC stretching band and C-O stretching band are observed at 1296.1 cm^{-1} in the FTRaman spectrum (About 14% of PED). Band observed at 1129 cm^{-1} in the FTIR spectrum is attributed to C-O stretching vibration.

4.4 .Thermo dynamical properties

By Born – Oppenheimer Approximation the total energy of a molecule can be expressed as the sum of translational, rotational, vibrational and electronic energies. That is

$E_{total} = E_{trans} + E_{rot} + E_{vib} + E_{ele} + \ldots\ldots\ldots$. It is assumed that for simplicity that the various types of energy associated with different motions of the molecule are independent of one another. On the basis of vibrational investigations at B3LYP/6-311++ G(d,p) basis set the statistical thermo chemical analysis of 2HBT is carried out considering the molecule to be at room temperature of 298.15 K and one atm pressure. The thermodynamic parameters like Zero Point Vibrational Energy (ZPVE) and rotational constants in G Hz of the title molecule were calculated and tabulated in Table 4.

Table 4 The calculated Thermodynamical parameters of 2HBT

Parameters	B3LYP/6-311++G(d,p)	
Zero-Point Vibrational	278.89 (kJ/Mol)	
Rotational constants (GHz):	A	2.89093
	B	0.91735
	C	0.69637

The variation of thermodynamic functions like heat capacity $\left(C^{0}_{p,m}\right)$, entropy $\left(S^{0}_{m}\right)$ and enthalpy changes $\left(H^{0}_{m}\right)$ for 2-Hydroxybenzothiaziole (2HBT) with different temperatures rangingfrom 100-1000K were calculated ,using THERMO.PL [K.K. Irikura,2002] .These calculated thermodynamic parameters for various ranges (100 - 1000K) of temperatures were presented in Table 5.

Table 5-The Temperature dependence of Thermodynamic parameters of 2HBT

Temperature [T] (K)	Heat capacity [Cp] (Cal/mol-Kelvin)	Entropy [S] (Cal/mol-Kelvin)	Enthalpy[H] (kJ/ mol)
100	55.9	268.93	4.06
200	98.54	320.43	11.74
298.15	141	367.79	23.52
300	141.76	368.67	23.78
400	179.33	414.77	39.9
500	209.36	458.15	59.4
600	232.71	498.48	81.55
700	250.98	535.78	105.77
800	265.57	570.28	131.62
900	277.44	602.27	158.79
1000	287.26	632.02	187.04

It is clear that from Table 6 all the thermodynamic functions are increasing with the temperature due to the fact that the molecular vibrational intensities are increasing with temperatures.The correlation equation among heat capacity, entropy, enthalpy changes with temperatures were fitted by quadratic

IJASRM
International Journal of Advanced Scientific Research and Management, Volume 3 Issue 8, Aug 2018
www.ijasrm.com
ISSN 2455-6378

formulas and the corresponding fitting factors (R^2) these thermodynamic properties are 0.99956, 0.99984 and 0.99938 respectively. The correlations plot of Heat Capacity with temperature of 2HBT is shown in Fig. 6 and those of Entropy with temperature and Enthalpy change with temperatures are respectively shown in fig 7 and Fig. 8 . The corresponding fitting equations are follows:

$\left(C_{p,m}^{0}\right) = 25.9038 + 0.6436T - 2.8331 \times 10^{-4}T^2$

($R^2 = 0.99956$)

$\left(S_{m}^{0}\right) = 258.885 + 0.7796T - 2.1163 \times 10^{-4}T^2$

($R^2 = 0.99984$)

$\left(H_{m}^{0}\right) = -8.2479 + 0.09863T - 1.6577 \times 10^{-4}T^2$

($R^2 = 0.99938$)

The thermodynamic functions grant very useful information for the further study on the 2HBT. They can be used to calculate the other thermodynamic energy according to the relationship of thermodynamic functions and evaluate directions of chemical behaviour according to the second law of thermodynamics in the thermochemical field [S. Muthu et al,2013]

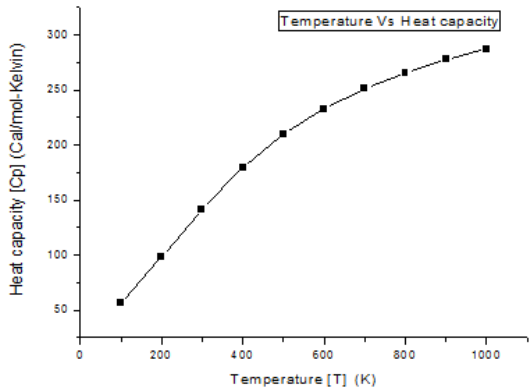

Fig. 6.Temperature dependence of Heat Capacity [Cv] of 2HBT

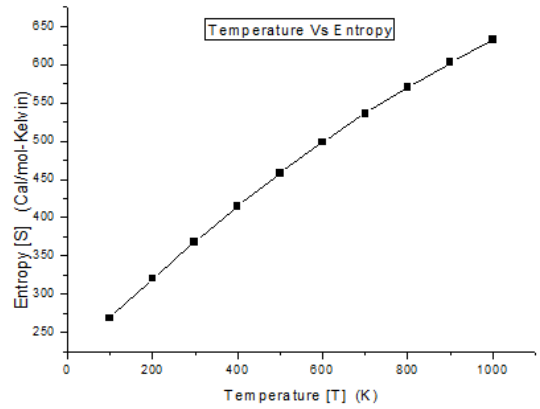

Fig. 7.Temperature dependence of Entropy [S] of 2HBT

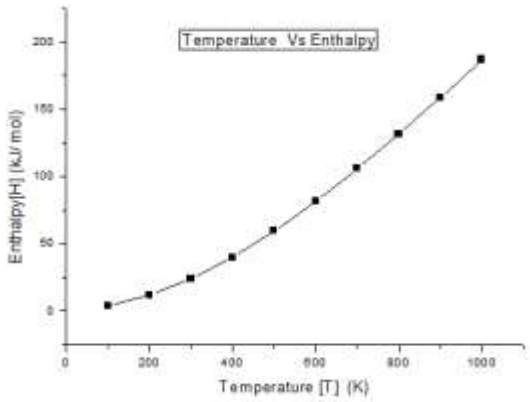

Fig. 8 Temperature dependence of Enthalpy[H] of 2HBT

It can be seen that, when the temperature increases from 100 to 1000 K the thermodynamic functions like Specific heat capacity at constant volume (C_V), Entropy(S) and enthalpy (ΔH) are also increases since molecular vibrational intensities increase with temperature [J.B. Ott et al,2000]. The entropy and enthalpy changes revealed that the title compound possesses more flexibility of changing its own thermodynamic system with respect to the temperature. Fitting factor of the thermodynamic functions such asEnergy , specific heat heat capacity at constant volume, entropy and enthalpy changes at room temperature are 107.278 kCal/mol 31.036 Cal/mol-Kelvin, 90.854 Cal/mol-Kelvin and 0.171908 kJ/mol respectively.

4.5. ^{13}C and ^{1}H NMR spectral analysis

The isotropic chemical shifts are frequently used as an aid in identification of reactive organic as well as ionic species. In general only nuclei with odd mass numbers are NMR active (^{1}H ,^{13}C ,^{19}F ,^{31}P etc) .The accuracy of NMR theoretical predictions depend on the implemented basis set and optimized structural parameters. Therefore, structural parameters obtained with the hybrid B3LYP functional at the 6-311++G(d,p) level of theory were used to predict ^{1}H and ^{13}C chemical shifts utilizing the recommended GIAO approach [H.O. Kalinowski et al 1988]. Chemical shifts were reported in parts per million relative to TMS (Tetramethylsilane). Relative chemical shifts were estimated by using the corresponding TMS shielding calculated in advance at the same theoretical level as the reference. It is recognized that accurate predictions of molecular geometries are essential for reliable calculations of magnetic properties [S. Sebastian et al ,2011] . The theoretical values for ^{1}H and ^{13}C NMR of 2HBT was given in Table 10. The correlation coefficient for proton chemical shifts is found to be 0.9991 and this value for carbon

IJASRM
International Journal of Advanced Scientific Research and Management, Volume 3 Issue 8, Aug 2018
www.ijasrm.com
ISSN 2455-6378

chemical shift is found to be 0.9969 by B3LYP method using the 6311++G(d,p) basis function. The H atom is the smallest of all atoms and mostly localized on the periphery of molecules. Therefore their chemical shifts would be more susceptible to intermolecular interactions in the aqueous solution as compared to that for other heavier atoms. Another important aspect is that, hydrogen attached or nearby electron withdrawing atom or group can decrease the shielding and move the resonance of attached proton towards a higher frequency. By contrast electron donating atom or group increases the shielding and moves the resonance towards to a lower frequency [S. Sebastian et al ,2011]. Aromatic carbons give signals in overlapped areas of the spectrum with chemical shift values from 100 to 150 ppm [H.O. Kalinowski etal 1988; K. Pihlajaet al 1994]. For 2HBT, ^{13}C NMR chemical shifts in the ring are >100 ppm (in Table 10), as they would be expected. Nitrogen ,Sulphur and oxygen atoms show electronegative property, therefore, the calculated chemical shift value of ^{13}C which is seated in five membered ring is 172.7583 ppm .The chemical shift of two carbon peaks C4 and C5 in the ring attached with Nitrogen and Sulphur respectively were calculated as 156.0889 ppm andb144.151 ppm. The theoretically computed ^{13}C and ^{1}H NMR spectrum are shown in Figure 9. The 2HBT has four hydrogen atoms attached to the carbons of aromatic ring and one hydrogen atom attached with oxygen atom in the alcohol group. The chemical shift values of H atom in alcohol group is quite low (≤5ppm) due to the shielding effect. The other four H atoms have a greater value around 7 to 8 ppm. The chemical shift values of all Carbon and Hydrogen atoms were reported in Table 6.

Table 6. Theoretical isotropic chemical shift calculated using DFT B3LYP/6-31 G(d,p) (with respect to TMS, All values in ppm) for 4A3NP

Calculated chemical shift (ppm)	
Atom	**B3LYP/6-31G(d,p)**
C2	172.7583
C4	156.0889
C5	144.1581
C6	124.4597
C7	127.5654
C8	130.5146
C9	127.3409
H10	7.8572
H11	7.4046
H12	7.2295
H13	7.6179
H15	4.9466

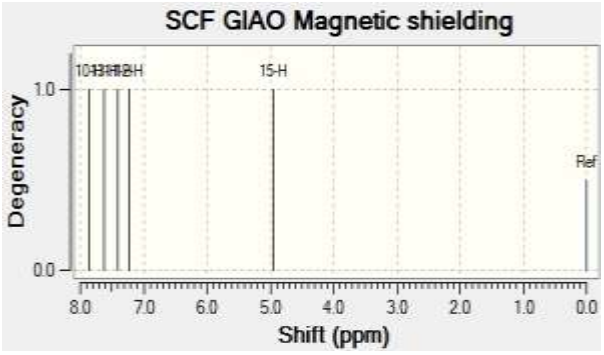

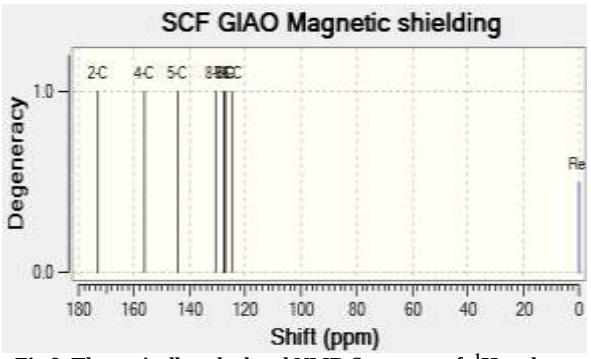

Fig 9. Theoretically calculated NMR Spectrum of ^{1}H and ^{13}C of 2HBT

4.6 Mullikkan Charges

The atomic charge in molecules is fundamental to chemistry. For instance, atomic charge has been used to describe the processes of electronegativity equalization and charge transfer in chemical reactions [K. Jug et al 1991; S. Fliszar et al ,1983] and to model the electrostatic potential outside molecular surfaces [P.E. Smith et al,1991; J. Gao ,1993; P. Cieplak ,1991]. Mullikan's population analysis provides [R.S. Mulliken,1995] partitioning of either a total charge density or an orbital density. Mullikan's atomic charges of 2HBT had been calculated by DFT method were shown in Table 7 The magnitude of the hydrogen atomic charges is found to be only positive and arranged in an order from 0.129 to 0.254 for DCT for 2HBT, indicating the charge transfer from H to carbon atom. Mulliken atomic charges calculated at the B3LYP/6-311G++g(d,p) method is collected in Table 7 along with the natural atomic charges obtained in NBO analysis.

Table 7.Atomic charges for optimized geometry of 4A3NP using DFT B3LYP/6-31g(d,p)

Atomic Number	Mulliken Atomic Charges
S1	-0.391
C2	0.215
N3	-0.001
C4	-1.497
C5	1.85

IJASRM
International Journal of Advanced Scientific Research and Management, Volume 3 Issue 8, Aug 2018
www.ijasrm.com
ISSN 2455-6378

C6	0.5
C7	-0.113
C8	-0.154
C9	-1.01
H10	0.132
H11	0.13
H12	0.129
H13	0.13
O14	-0.175
H15	0.254

It is clear from the table that that C2 ,C5 and C6 atoms of 2HBT exhibit positive charge, while C4,C7,C8 and C9 atoms exhibit negative charges. C4 atom has a maximum negative charge value of about −1.497. The maximum positive atomic charge is obtained for C5 having a charge value about 1.851 which is a carbon atom present in both of the ring. However all the hydrogen atoms exhibit a net positive charge. Of which H15 connected with O in the alcohol group has maximum charge value about 0.254. This is due to the reason of electro negative oxygen of the OH group. Illustration of Mullikan atomic charges was plotted at 6-311++g(d,p) level have been shown in Figure 10 .The presence of large negative charge on S and O atoms and net positive charge on H atom may suggest the formation of intramolecular interaction in solid forms.

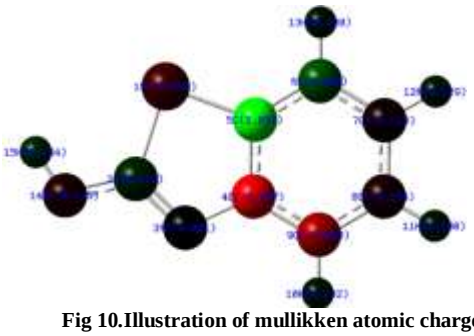

Fig 10.Illustration of mullikken atomic charges

4.7. Donor- acceptor interactions

The NBO analyzes aid and more efficient method for studying intra and inter molecular bonding and interaction among bonds, and also provides a convenient basis for inspecting charge transfer or conjugative interactions in the molecular system. Some electron donor orbital, acceptor orbital and the overlap stabilization energy resulting from the second-order micro-disturbance theory are reported [R. Srinivasaraghavan et al,2015; C. James et al ,2006; J. Liu et al , 2005]. NBO studies give the most precise possible 'natural Lewis structure' picture because all orbital details are mathematically chosen to include the highest possible percentage of the electron density. For each donor (i) and acceptor (j), the stabilization energy E(2) associated with the delocalization i, j estimated as

$$E_2 = \Delta E_{ij} = q_i \frac{F(i,j)^2}{E_i - E_j} \qquad (4)$$

Where q_i is the donor orbital occupancy, E_i and Ej are diagonal elements and F(i,j) is the off diagonal NBO Fock matrix elements.

Table 8 Second order perturbation theory analysis of Fock matrix in NBO basis for 2HBT

Donour NBO (i)	Type	ED/e (Occupancy)	Acceptor NBO (j)	Type	ED/e (Occupancy)	[a]E(2) k cal/mol	[b]E(j)-E(i) a.u	[c]F(i,j) a.u
SI-C2	σ	1.9812	C5-C6	σ*	0.56397	4.34	1.23	0.065
S1-C5	σ	1.97562	C2-O14	σ*	0.33248	4.33	1.01	0.059
C2-N3	π	1.89857	C4-C5	π*	0.00335	16.22	0.35	0.075
N3-C4	σ	1.97231	C2-O14	σ*	0.33248	7.19	1.12	0.08
C4-C5	π	1.64337	C6-C7	π*	0.02065	20.17	0.3	0.069
C4-C6	π	2.64337	C8-C9	π*	0.02767	16.21	0.3	0.063
C4-C9	σ	1.97109	C4-C5	σ*	0.52678	4.73	1.24	0.068
C6-C7	σ	1.97135	S1-C5	σ*	0.18477	6.25	0.89	0.067
C6-C7	π	1.69283	C4-C5	π*	0.00335	18.75	0.27	0.066
C6-C7	π	1.69283	C8-C9	π*	0.02767	19.17	0.29	0.067
C8-C9	π	1.69062	C4-C5	π*	0.00335	21.87	0.26	0.07
C8-C10	π	1.69062	C6-C7	π*	0.02065	19.85	0.28	0.067
S1	LP(2)	1.72744	C2-N3	π*	-0.01649	24.83	0.25	0.072
S2	LP(2)	2.72744	C4-C5	π*	0.00335	15.99	0.27	0.062
N3	LP(1)	1.86921	S1-C2	σ*	0.13825	18.22	0.51	0.086
O14	LP(2)	1.85206	C2-N3	π*	0.33248	35.82	0.34	0.104

[a]E(2) means energy of hyper conjugative interaction (stabilization energy)
[b]Energy difference between donor and acceptor i and j NBO orbitals.
[c]F(i,j) is the Fock matrix element between i and j NBO orbitals

The second order fock matrix was carried out to evaluate the donor-acceptor interactions in the NBO analysis [M. Szafran et al, 2007]. The higher the E(2) value, the molecular interaction between electron donors and electron acceptors is more intensive and the greater the extent of conjugation of the entire system . Delocalization of electron density amid occupied Lewis-type (bond or lone pair) NBO orbitals and properly unoccupied (antibond or Rydgberg) non-Lewis NBO orbitals resemble to a stabilizing donor-acceptor interaction. NBO analysis has been performed on the 2HBT molecule at the B3LYP/6-311++G(d,p) level in order to elucidate the intra molecular, rehybridization and delocalization of electron density within the molecule. The strong intramolecular hyper conjugative interaction of the σ and π electrons of C - C to the anti C - C bond of the ring leads to stabilization of some part of the ring as evident from Table 8. Here for our title compound, several types of electronic interactions available between bonding, non-bonding and anti-bonding orbitals. In the case of 2HBT the highest stabilization about 26.23 kJ/mol is observed at the interaction between Lone Pair LP(2) (O14) $\rightarrow \pi^*$ (C2-N3). The $\pi \rightarrow \pi^*$ type of transition was observed at the interaction between C8$\rightarrow$ C9 and C4$\rightarrow$ C5 and with stabilization energy is about 21.87 kJ/mol.

5. Conclusion

A complete structural information , FT-IR and FT-Raman vibrational analysis ,electronic properties and vibrational properties of 2HBT have been carried out with the help of DFT calculations at B3LYP/6-311+ g(d,p) level. The MESP map shows that the negative potential sites are around Nitrogen and Oxygen atoms and the positive potential sites are mainly around the hydrogen atoms. The vibrational frequencies, infrared intensities Raman activities and Raman intensities of 2HBT were calculated. The theoretically calculated vibrational modes are compared with experimental values. The experimental values are in good agreement with theoretical values. The difference between the observed and scaled wavenumber values of most of the fundamentals is very small. The thermodynamic properties (heat capacity at constant volume, entropy and enthalpy changes) in the temperature ranges from 100 to 1000 K ,Rotational constants, a zero point vibrational energy and SCF energy of title compound were calculated. The ^{1}H and ^{13}C NMR magnetic isotropic chemical shifts were calculated by B3LYP/6-311++ g(d,p) basis set . Rotational constants, zero point vibrational energy and SCF energy of title compound were calculated. Mullikan atomic charges were listed and the hyper conjugative interaction energy and electron densities of the donor and acceptor bond of title compound were studied by NBO analysis

Acknowledgement

The authors are thankful to Sophisticated Analytical Instrumentation Facility (SAIF), IIT, Chennai, for the spectral measurements.

REFERENCE

[1] Mansingh, J. Chem. Phys. 52 (1970) 5896–5901.
[2] A.E. Reed, F. Weinhold, J. Chem. Phys. 83 (1985) 1736–1740.
[3] A.P. Datin, J.M. Lebas, Spectrochim. Acta A 25 (1969) 168–185.
[4] James, A. Amal Raj, R. Reghunathan, V.S. Jayakumar, I.Hubert Joe, Structural conformation and vibrational spectroscopic studies of 2,6-bis(p-N,N-dimethyl benzylidene) cyclohexanone using density functional J. Raman Spectrosc. 37 (2006) 1381-1392.
[5] F.J. Luque, J.M. Lopez, M. Orozco, Theor. Chem. Acc. 103 (2000) 343–345.
[6] G. Keresztury, in: J.M. Chalmers, P.R. Griffth (Eds.), Raman Spectroscopy: Theory in Handbook of Vibrational Spectroscopy, vol. 1, John Wiley & Sons Ltd., New York, 2002, pp. 71–87
[7] G. Keresztury, S. Holly, G. Besenyei, J. Varga, A. Wang, J.R. Durig, Spectrochim. Acta 49 (1993) 2007–2026.
[8] George Socrates, Infrared and Raman Characteristics Group Frequencies -Tables and Charts, third ed., John Wiley and Sons, New York, 2001.
[9] H.O. Kalinowski, S. Berger, S. Braun, Carbon-13 NMR Spectroscopy, John Wiley&Sons, Chichester, 1988.
[10] Hans-Wilhelm Engels, Herrmann-Josef Weidenhaupt, Manfred Pieroth, Werner Hofmann, Karl-Hans Menting, Thomas Mergenhagen, Ralf Schmoll, Stefan Uhrlandt "Rubber, 4. Chemicals and Additives" in Ullmann's Encyclopedia of Industrial Chemistry 2004, Wiley-VCH, Weinheim.
[11] Hrobarik, P.; Sigmundova, I.; Zahradnik, P.; Kasak, P.; Arion, V.; Franz, E.; Clays, K. (2010). "Molecular Engineering of Benzothiazolium Salts with Large Quadratic Hyperpolarizabilities: Can Auxiliary Electron-Withdrawing Groups Enhance Nonlinear Optical Responses?". Journal of Physical Chemistry C. 114 (50): 22289–22302
[12] J. Gao, J. Chem. Phys. 98 (1993) 1975–1981.
[13] J. Liu, Z. Chen, S. Yuan, Study on the prediction of visible absorption maxima of azobenzene compounds, J. Zhejing Univ. Sci B. 6 (2005) 584-589.
[14] J.B. Ott, J. Boerio-Goates, Chemical Thermodynamics: Advanced Applications, Calculations from Statistical Thermodynamics, Academic Press 2000.

[15] J.M. Seminario, Recent Developments and Applications of Modern Density Functional Theory, vol. 4, Elsevier, Amsterdam, 1996.
[16] K. Jug, Z.B. Maksic, in: Z.B. Maksic (Ed.), Theoretical Model of Chemical Bonding, Part 3, Springer, Berlin, 1991, p. 233.
[17] K. Pihlaja, E. Kleinpeter (Eds.), Carbon-13 Chemical Shifts in Structural and Sterochemical Analysis, VCH Publishers, Deerfield Beach, 1994.
[18] K.K. Irikura, THERMO.PL, National Institute of Standards and Technology, Gaithersburg, MD, 2002.
[19] L. Verdonck, G.P. Vander Kelen, Spectrochim. Acta A 28 (1972) 55–57.
[20] L. Verdonck, G.P. Vander Kelen, Z. Eeckhant, Spectrochim. Acta A 29 (1973) 813–816.
[21] Lucille Le Bozec, Christopher J. Moody "Naturally Occurring Nitrogen–Sulfur Compounds. The Benzothiazole Alkaloids" Australian Journal of Chemistry 62(7) 639–647.
[22] M. Arivazhagan, V. Krishna Kumar, R. John Xavier, G. Ilango and V. Balachandran, Spectrochim. Acta, A72 (2009)941-946.
[23] M. J. Frisch, G. W. Trucks, H. B. Schlegel, G. E. Scuseria, M. A. Robb, J. R. Cheeseman, G. Scalmani, V. Barone, B. Mennucci, G. A. Petersson, H. Nakatsuji, M. Caricato, X. Li, H. P. Hratchian, A. F. Izmaylov, J. Bloino, G. Zheng, J. L. Sonnenberg, M. Hada, M. Ehara, K. Toyota, R. Fukuda, J. Hasegawa, M. Ishida, T. Nakajima, Y. Honda, O. Kitao, H. Nakai, T. Vreven, J. A. Montgomery, Jr., J. E. Peralta, F. Ogliaro, M. Bearpark, J. J. Heyd, E. Brothers, K. N. Kudin, V. N. Staroverov, R. Kobayashi, J. Normand, K. Raghavachari, A. Rendell, J. C. Burant, S. S. Iyengar, J. Tomasi, M. Cossi, N. Rega, J. M. Millam, M. Klene, J. E. Knox, J. B. Cross, V. Bakken, C. Adamo, J. Jaramillo, R. Gomperts, R. E. Stratmann, O. Yazyev, A. J. Austin, R. Cammi, C. Pomelli, J. W. Ochterski, R. L. Martin, K. Morokuma, V. G. Zakrzewski, G. A. Voth, P. Salvador, J. J. Dannenberg, S. Dapprich, A. D. Daniels, Ö. Farkas, J. B. Foresman, J. V. Ortiz, J. Cioslowski, and D. J. Fox, Gaussian 09, Revision E.01, Gaussian, Inc., Wallingford CT, 2009.
[24] M. Silverstein, G. Clayton Basseler, C. Morill, Spectrometric Identification of Organic Compound, Wiley, New York, 1981.
[25] M. Szafran, A. komasa, E.B. Adamska, Crystal and molecular structure of 4-carboxypiperidinium chloride (4-piperidinecarboxylic acid hydrochloride), J Mol. Struct. THEOCHEM 827 (2007) 101-107.
[26] N. Sundaraganesan, Dominic Joshua, C. Meganathan & S. Sebastian, Indian J.Chem, Sec A (47A) (2008) 821-829.
[27] N.B. Colthup, L.H. Daly, S.E. Wiberley, Introduction to Infrared and Raman Spectroscopy, Academic Press, New York, 1964. pp. 226;
[28] P. Cieplak, J. Comp. Chem. 12 (1991) 1232–1236.
[29] P.E. Smith, J. Am. Chem. Soc. 113 (1991) 6029–6037.
[30] Roy Dennington, Todd Keith, and John Millam, GaussView, Version 5, Semichem Inc., Shawnee Mission, KS, 2009.
[31] R.Srinivasaraghavan, S. Thamaraikannan, S. Seshadri, T. gnanasambandan, Molecular conformational stability and Spectroscopic analysis of Parared with experimental techniques and quantum chemical calculations, Spectrochim. Acta A 137 (2015) 1194-1205.
[32] R.H. Petrucci, W.S. Harwood, F.G. Herring, J.D. Madura, General Chemistry: Principles & Modern Applications, ninth ed., Pearson Education Inc., New Jersey, 2007.
[33] R.J. Jakobsen, F.F. Bentley, Appl. Spectrosc. 18 (1964) 88–92.
[34] R.S. Mulliken, J. Chem. Phys. 23 (1995) 1833–1840.
[35] S. Chidangil, M.K. Shukla, P.C. Mishra, J. Mol. Model. 4 (1998) 250–258.
[36] S. Fliszar, Charge Distributions and Chemical Effects, Springer, New York, 1983.
[37] S. Muthu, E. Isac Palulraj, Spectroscopic and molecular structure (monomeric and dimeric structure) investigation of 2-[(2-hydroxyphenyl) carbonyloxy] benzoic acid by DFT method: A combined experimental and theoretical study, J. Mol. Struct 1038 (2013) 145-162.
[38] S. Sebastian, N. Sundaraganesan, B. Karthikeiyan, V. Srinivasan, Spectrochim. Acta Part A 78 (2011) 590–600.
[39] T. E. Gilchrist "Heterocyclic Chemistry" 3rd Edition, Longman, 1992.
[40] T. Sundius, J. Mol. Struct. 218 (1990) 321–326.
[41] T. Sundius, Vib. Spectrosc. 29 (2002) 89–95.
[42] V. Balachandran, A. Lakshmi, A. Janaki, J. Mol. Struct. 1013 (2012) 75–85.
[43] Y. Sheena Mary a, C. Yohannan Panicker b, M. Sapnakumari c, B. Narayana c, B.K. Sarojini d, Abdulaziz A. Al-Saadi e, Christian Van Alsenoy f, Javeed Ahmad War g Spectrochimica Acta Part A: Molecular and Biomolecular Spectroscopy 138 (2015) 73–84